FTIR Studies of CO Adsorption on Al_2O_3- and SiO_2-Supported Ru Catalysts

Soo Yin Chin, Christopher T. Williams, and Michael D. Amiridis*

Department of Chemical Engineering, University of South Carolina, Columbia, South Carolina 29208

Received: July 15, 2005; In Final Form: November 7, 2005

The adsorption of CO on Al_2O_3- and SiO_2-supported Ru catalysts has been investigated through FTIR spectroscopy. Deconvolution of the spectra obtained reveals the presence of 11 distinct bands in the case of Ru/Al_2O_3 and 10 bands in the case of Ru/SiO_2, which were assigned to different carbonyl species adsorbed on reduced as well as partially oxidized Ru sites. Although most of these bands on both supports are similar, they exhibit substantial differences in terms of stability. In general, the analogous CO species on Ru/Al_2O_3 are adsorbed stronger than those on Ru/SiO_2, with the most stable species observed being a dicarbonyl adsorbed on metallic Ru (i.e., $Ru^0(CO)_2$). Following sintering of the Ru, the ratio of multicarbonyl to monocarbonyl adsorption is reduced substantially because of the lack of isolated sites or small Ru clusters that enable the formation of multicarbonyl species via oxidative disruption. Finally, in the presence of O_2, the main features observed correspond to monocarbonyl, dicarbonyl, and tricarbonyl species adsorbed on partially oxidized Ru^{n+}. The intensities of all bands decrease drastically at temperatures above 210 °C because of the onset of CO oxidation, which results in substantially reduced surface coverage.

1. Introduction

Infrared spectroscopic studies of adsorbed CO represent an effective tool for probing the surface structure of supported metal catalysts. Such studies have been performed on various metals,[1] and in some cases (e.g., platinum) the CO adsorption behavior is very well understood. On supported ruthenium catalysts, however, the results obtained during the adsorption of CO are much more complicated because of the presence of several different CO species on different types of reduced and partially oxidized Ru sites, making the interpretation of the spectra observed more difficult than with most other metals.

Most previous literature reports agree that upon CO adsorption on supported Ru catalysts characteristic absorption bands appear in the spectra in three different regions: HF_1 (high-frequency 1) at 2120−2156 cm^{-1}, HF_2 at 2060−2110 cm^{-1}, and LF (low frequency) at 2000−2060 cm^{-1}.[2] Analysis of the available literature data indicates that there are at least three different types of adsorbed CO species associated with these bands: type I carbonyls (i.e., Ru^0-CO), which are characterized by an LF band;[3−6] type II carbonyls (i.e., $Ru^{n+}(CO)_x$), which are characterized by an HF_1-HF_2 set of bands, with the exact values of n and x under debate;[7−13] and type III carbonyls (i.e., $Ru^{n+}(CO)_2$), which are characterized by an HF_2-LF set of bands.[10,12−18] As a result, the nature of the bands in the HF_2 region is fairly complex because of contributions from several different species. Furthermore, it has been reported that the intensity of the HF_2 bands is enhanced in the presence of O_2, leading to the hypothesis that some contributions in this region can be assigned to monocarbonyl species adsorbed on $Ru^{\delta+}$.[7,19] Notwithstanding these previous studies, some of the band assignments remain controversial. One of the main problems has been the deconvolution of low-intensity bands among more intense ones in the same spectral regions.

In this paper, we report the results of a systematic FTIR spectroscopic study of the adsorption of CO on Ru/SiO_2 and Ru/Al_2O_3 at various temperatures up to 300 °C. Thermal desorption experiments were also performed to reduce the surface coverage of different species and allow identification of some lower intensity overlapping bands in the spectra. The spectra were then deconvoluted in an effort to understand the adsorption behavior of CO on these supported Ru catalysts. The adsorption of CO was also performed on sintered samples, which are expected to exhibit different ratios of mono- to multicarbonyl species because of steric hindrances, as well as in the presence of O_2, which is expected to change the ratio of Ru^{n+} to Ru^0 sites on the catalyst surface. Simultaneous analysis of all of the spectra obtained from samples with different supports, Ru particle sizes, and oxidation states allows us to assign the various bands observed with a high degree of confidence.

2. Experimental Section

2.1. Catalyst Preparation. Supported Ru catalysts with nominal metal loadings of 1.0 wt % (ICP measurements, Galbraith Laboratory) were prepared via incipient wetness impregnation onto SiO_2 (Grace Davison, XPO-2301, 300 m^2/g) and γ-Al_2O_3 (Degussa, Alumina C, 100 m^2/g) supports using ruthenium nitrosylnitrate ($Ru(NO)(NO_3)_3 \cdot xH_2O$, Alfa Aesar) as the precursor. Prior to impregnation, both supports were calcined overnight at 500 °C. Following impregnation, all catalysts were dried overnight at 120 °C and reduced at 300 °C in 5% H_2/N_2 for 2 h (H_2). For comparison purposes, experiments were also conducted with an Ru/Al_2O_3 sample that underwent a oxidation treatment at 300 °C in 5% O_2/N_2 for 2 h prior to a reduction step at 300 °C in 5% H_2/N_2 for 2 h (O_2-H_2). The temperature ramp used in all cases was 3 °C/min. The structures of these catalysts upon treatment under the above conditions have been characterized in detail, and the results have been reported elsewhere.[20]

2.2. Fourier Transform Infrared (FTIR) Spectroscopic Studies of Adsorbed CO. Transmission FTIR spectra were collected in the single beam mode, with a resolution of 2 cm^{-1} using a Nicolet Nexus 470 spectrometer equipped with a MCT-B

* Corresponding author: E-mail: amiridis@engr.sc.edu.

10.1021/jp053908q CCC: $33.50
Published on Web 12/17/2005

detector cooled by liquid nitrogen. A stainless steel cell (10 cm long) with both ends "capped" by IR-transparent NaCl windows cooled by flowing water was used in the experiments. The cell was wrapped with a heating element to allow spectra to be collected at elevated temperatures, while the temperature was monitored by a thermocouple placed in close proximity to the catalyst samples. Reference spectra of the clean surfaces in He were collected at different temperatures as needed.

Samples were pressed into thin self-supported disks with a diameters of 12 mm and "thicknesses" of approximately 20 mg/cm^2. Prior to each experiment, the sample used was pretreated in situ according to one of the activation protocols described above. The sample was then cooled to room temperature in flowing He, and a mixture of 1% CO/He, purified by passage through oxygen and water traps, was introduced into the cell, with spectra collected at different time intervals until a steady state was reached (approximately 90−120 min). Subsequently, the cell was heated at intervals of 40−60 °C and spectra were collected in flowing 1% CO/He at each temperature. Alternatively, following the adsorption of CO at room temperature, helium was purged through the cell, with spectra collected until no further changes were observed. The cell was then heated in flowing He at intervals of 40−60 °C, and spectra were collected at each temperature to monitor the desorption behavior of the adsorbed CO. To examine the effect of O_2, spectra were also collected at different temperatures in a 0.5% CO−0.5% O_2/He flowing mixture.

Spectral deconvolution and fitting was performed using the Galactic PeakSolve peak-fitting software. This software allows for the fitting of the observed spectra using peaks with an array of different shapes (i.e., Gaussian, Lorentzian, log-normal, etc.) and variable peak height, width, and position. In general, the weaker bands at lower wavenumbers (i.e., 1700−1900 cm^{-1}) were fitted using Gaussian peaks, the bands exhibiting visible asymmetric tailing were fitted using log-normal peaks, and all other bands were fitted with peaks of a mixed Gaussian−Lorentzian type. Curve-fitting for all sets of spectra was performed starting with the spectra collected under conditions of the lowest surface coverage. Subsequently, using the same set of parameters the spectra collected under conditions of the higher surface coverage were fitted with a similar set of constraints imposed on the parameters, such as peak width, fwhm, and percent of Lorentzian. All of the deconvoluted spectra shown in this paper are converged solutions, with correlation factors above 0.999 and standard errors below 0.002.

3. Results

3.1. CO Adsorption at Room Temperature. *3.1.1. Highly Dispersed Samples.* A. Ru/Al_2O_3. Spectra collected following adsorption of CO at room temperature on Ru/Al_2O_3 pretreated in H_2 and subsequent desorption in He are shown in Figure 1. At room temperature, the adsorbed CO remained strongly bonded on the surface, and two main features were observed in the spectrum: a relatively weak band centered at 2141 cm^{-1} in the HF_1 region and a broad and strong band in the 1900−2120 cm^{-1} region, which evidently consists of several overlapping bands with local peaks and shoulders at approximately 2038, 2061, 2070, and 2108 cm^{-1} as well as substantial tailing in the 1950 cm^{-1} region. In addition, a very weak and broad band is also observed in the 1800 cm^{-1} region. As the desorption temperature increased, the band at 2038 cm^{-1} underwent a red shift accompanied by a rapid decrease in intensity and eventually became a shoulder of the stronger bands in the region at temperatures above 150 °C. Similarly, the intensities of the shoulders at 2070 and 2108 cm^{-1} decreased with increasing desorption temperature, although a shift was not apparent in this case because the spectra were poorly resolved in this region. At temperatures above 110 °C, the shoulder at 2108 cm^{-1} disappeared completely, while the shoulder at 2070 cm^{-1} remained visible up to 250 °C. In contrast, in the region below 2000 cm^{-1}, two bands at approximately 2005 and 1975 cm^{-1} appear to develop and become discernible with increasing temperature. As a result, at 150 °C, the HF_2 and LF regions have changed completely and are dominated by three main bands at 2050, 2005, and 1976 cm^{-1} and a very weak shoulder at 2077 cm^{-1}. Nevertheless, the results of spectral fitting reveal that the strong band that originally appears at 2038 cm^{-1} at room temperature is still present up to 210 °C but at a lower intensity (Figure 2). Further increase of the temperature resulted in the parallel decrease in intensity of all bands. Consequently, at 300 °C only three bands at 2049, 2001, and 1970 cm^{-1} remained in the spectrum with tailing observed at lower frequencies and a possible shoulder at 1943 cm^{-1}. These results are consistent with previous literature reports.[21,22]

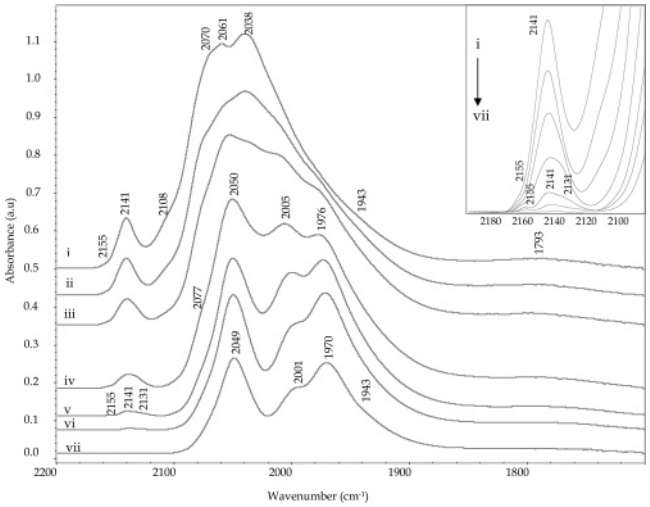

Figure 1. FTIR spectra collected following adsorption of CO at room temperature on Ru/Al_2O_3 pretreated in H_2 at 300 °C and subsequent desorption in He at (i) 25, (ii) 70, (iii) 110, (iv) 150, (v) 210, (vi) 250, and (vii) 300 °C. The insert shows magnification of the HF_1 region.

In the HF_1 region, the intensity of the band at 2141 cm^{-1} also decreased relatively quickly with increasing temperature. Although this band appears to represent a single peak, an enlargement of the region (insert of Figure 1) clearly shows a weak shoulder at 2155 cm^{-1} in the room-temperature spectrum. At temperatures above 150 °C, a shoulder at 2131 cm^{-1} also becomes discernible. Both shoulders at 2131 and 2155 cm^{-1} are more stable with respect to temperature than the main band at 2141 cm^{-1}. Finally, the positions of all three features in this region are independent of surface coverage.

Overall, 10 bands ranging in frequency from 1700 to 2160 cm^{-1} can be observed in the spectra of Figure 1. Consequently, the spectra were fitted using these bands, as shown in Figure 2, with the corresponding peak positions and absolute and relative areas summarized in Table 1. The use of an additional broad band centered at 1950 cm^{-1} was necessary to successfully curve-fit the spectra because of the substantial asymmetric tailing observed in the low wavenumber region.

B. Ru/SiO_2. Spectra collected following adsorption of CO at room temperature on a Ru/SiO_2 sample pretreated in H_2 and subsequent desorption in He are shown in Figure 3. At room temperature, the adsorbed CO remained strongly bonded on the surface, and two main features were observed in the spectrum:

TABLE 1: Characteristic Frequencies and Peak Areas of Spectral Features Observed Following the Room Temperature Adsorption of CO on Ru/Al_2O_3 (Pretreated in H_2 at 300 °C) and Subsequent Desorption in He at Different Temperatures

temperature (°C)	1[a]	2[a]	3[b]	4[c,d]	5[e]	6[b]	7[c,f,g]	8[f]	9[g]	10[g]	11[f]
25	1789	1959	1990	2015	2038	2062	2080	2107	2130	2141	2154
absolute area (au)	3.99	10.09	9.39	10.98	14.35	12.85	10.94	2.19	0.44	2.08	0.11
relative area (%)	5.2	13.0	12.1	14.2	18.5	16.6	14.1	2.8	0.6	2.7	0.1
70	1793	1955	1987	2012	2037	2059	2079	2104	2132	2142	2155
absolute area (au)	3.84	12.24	11.05	11.35	11.95	12.88	7.15	1.34	0.52	1.28	0.06
relative area (%)	5.2	16.6	15.0	15.4	16.2	17.5	9.7	1.8	0.7	1.7	0.1
110	1792	1954	1984	2011	2035	2058	2078	2102	2132	2142	2155
absolute area (au)	3.87	14.02	12.02	11.79	9.7	13.22	5.14	0.47	0.47	0.86	0.06
relative area (%)	5.4	19.6	16.8	16.5	13.5	18.5	7.2	0.7	0.7	1.2	0.1
150	1780	1951	1980	2007	2027	2051	2075		2131	2141	
absolute area (au)	3.47	14.98	14.05	10.69	6.01	14.89	4.25		0.30	0.45	
relative area (%)	5.0	21.7	20.3	15.5	8.7	21.5	6.1		0.4	0.6	
210	1791	1952	1979	2005	2025	2050	2076		2132	2141	
absolute area (au)	4.6	13.69	13.77	7.53	3.74	13.97	1.7		0.10	0.13	
relative area (%)	7.8	23.1	23.2	12.7	6.3	23.6	2.9		0.2	0.2	
300	1800	1942	1970	2000		2049					
absolute area (au)	1.29	4.57	7.3	4.64		9.46					
relative area (%)	4.7	16.8	26.8	17.0		34.7					

[a] Bridge-bonded CO, $[Ru_2-(CO)]$. [b] Dicarbonyl CO species on Ru^0, $[Ru^0-(CO)_2]$. [c] Dicarbonyl CO species on Ru^{2+}, $[Ru^{2+}-(CO)_2]$. [d] Linearly adsorbed CO on high energy defects sites and/or isolated Ru^0 species surrounded by partially oxidized Ru, $[Ru^0-CO]$. [e] Linearly adsorbed CO on Ru^0, $[Ru^0-CO]$. [f] Linearly adsorbed CO on Ru^{n+}, $[Ru^{n+}-CO]$. [g] Tricarbonyl CO species on Ru^{n+}, $[Ru^{n+}(CO)_3$, $n = 1-3]$.

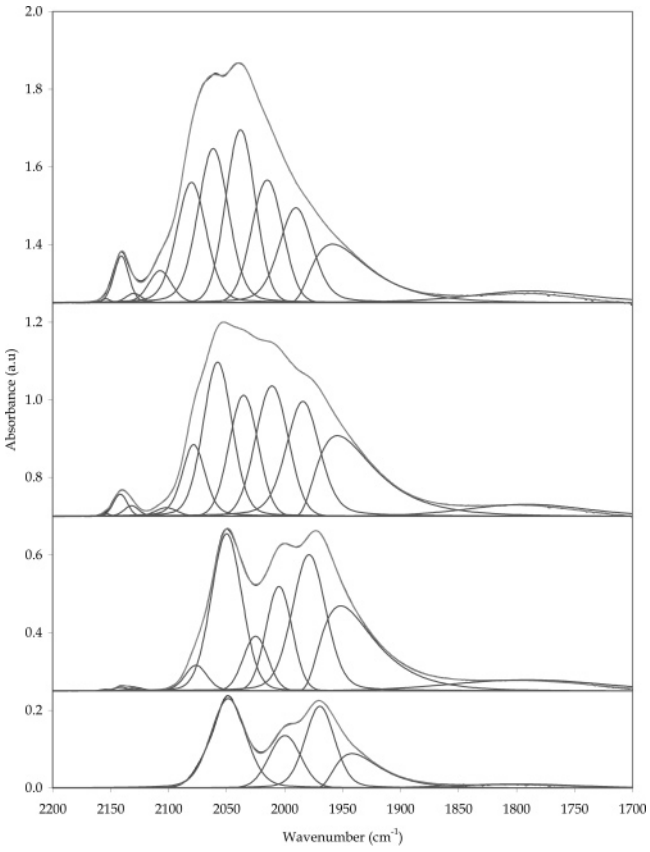

Figure 2. Fitting of selected spectra (i.e., from top to bottom i, iii, v, and vi) from Figure 1.

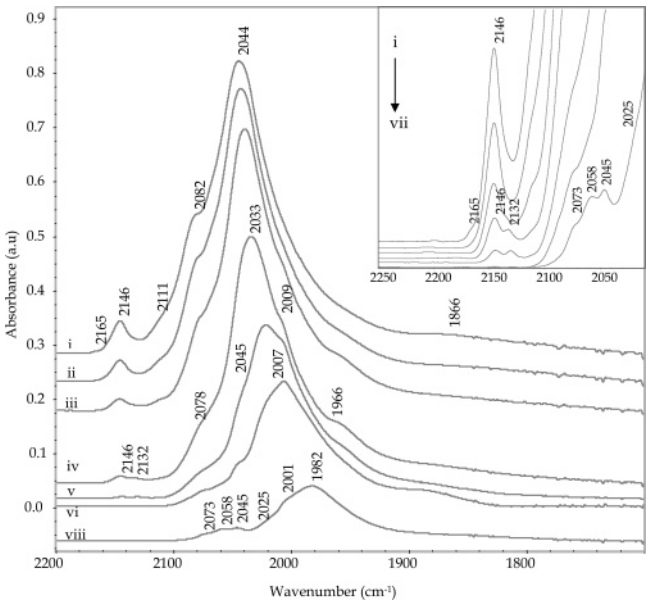

Figure 3. FTIR spectra collected following adsorption of CO at room temperature on Ru/SiO_2 pretreated in H_2 at 300 °C and subsequent desorption in He at (i) 25, (ii) 70, (iii) 110, (iv) 150, (v) 210, (vi) 250 and (vii) 300 °C. The insert shows magnification of the HF_1 region.

a relatively weak band in the HF_1 region centered at 2146 cm^{-1} and a broad and strong band in the 1900−2120 cm^{-1} region, which actually consists of a strong band centered at 2044 cm^{-1} with additional shoulders at 2082 and 2111 cm^{-1}. Finally, a very weak and broad band is also observed in the lower wavenumber region (1800−1900 cm^{-1}). As the temperature increased, the intensities of the stronger band at 2044 cm^{-1} and the shoulders at 2082 and 2111 cm^{-1} decreased, while their band positions were red-shifted. With the substantial decrease in intensity of the band at 2044 cm^{-1}, a shoulder at 2010 cm^{-1} and a band at approximately 1966 cm^{-1} became prominent at temperatures above 110 °C. Further decrease in intensity of the 2044 cm^{-1} band led to the emergence of an additional shoulder at approximately 2045 cm^{-1} at 210 °C, which was not discernible at lower temperatures. This shoulder undergoes a continuing red shift to 2025 cm^{-1} as the surface coverage decreased with increasing temperature up to 300 °C. Furthermore, at 250 °C the dominant band originally at 2044 cm^{-1} was reduced to a shoulder of the band at 2007 cm^{-1}. Further increase in temperature to 300 °C resulted to a further shift of these bands to 2001 and 1982 cm^{-1}, respectively. Finally, similar to what observed with Ru/Al_2O_3, the weak shoulder at 2111 cm^{-1} disappeared completely at temperatures above 110 °C.

Enlargement of the HF_1 region (insert of Figure 3) shows that the HF_1 band observed consists of three distinct features. The band at 2146 cm^{-1}, which is dominant, a shoulder at 2165 cm^{-1}, which is present only at room temperature, and an

TABLE 2: Characteristic Frequencies and Peak Areas of Spectral Features Observed Following the Room Temperature Adsorption of CO on Ru/SiO_2 (Pretreated in H_2 at 300 °C) and Subsequent Desorption in He at Different Temperatures

temperature/band (°C)	1[a]	2[a]	3[b,c]	4	5[d]	6[b]	7[e,f]	8[e]	9[f]	10[f]	11[e]
25	1866	1988	2020		2043	2063	2086	2111	2131	2146	2165
absolute area (au)	2.31	10.85	8.04		11.59	7.12	5.72	1.07	0.21	0.85	0.07
relative area (%)	4.8	22.7	16.8		24.2	14.9	12.0	2.2	0.4	1.8	0.1
70	1869	1985	2017		2041	2061	2083	2110	2133	2147	
absolute area (au)	1.57	9.48	7.69		11.58	6.78	5.00	0.49	0.19	0.19	
relative area (%)	3.6	22.1	17.9		26.9	15.8	11.6	1.1	0.4	0.4	
110	1883	1972	2014		2037	2053	2078	2109	2130	2146	
absolute area (au)	1.78	7.09	8.81		10.22	6.58	4.19	0.34	0.19	0.30	
relative area (%)	4.5	18.0	22.3		25.9	16.6	10.6	0.9	0.5	0.8	
150	1890	1970	2011		2033	2044	2070		2132	2146	
absolute area (au)	2.47	6.95	8.30		7.49	6.09	4.39		0.07	0.17	
relative area (%)	6.9	19.3	23.1		20.8	16.9	12.2		0.2	0.5	
210	1898	1972	2008		2028	2045	2068		2131	2144	
absolute area (au)	2.22	6.48	7.08		6.86	2.11	1.91		0.02	0.04	
relative area (%)	8.3	24.3	26.5		25.7	7.9	7.1		0.1	0.1	
300		1953	1978		2002	2025	~2060				
absolute area (au)		1.56	3.07		1.77	0.29	0.66[g]				
relative area (%)		21.2	41.8		24.1	3.9					

[a] Bridge-bonded CO, $[Ru_2-(CO)]$. [b] Dicarbonyl CO species on Ru^0, $[Ru^0-(CO)_2]$. [c] Linearly adsorbed CO on high energy defects sites and/or isolated Ru^0 species surrounded by partially oxidized Ru, $[Ru^0-CO]$. [d] Linearly adsorbed CO on Ru^0, $[Ru^0-CO]$. [e] Linearly adsorbed CO on Ru^{n+}, $[Ru^{n+}-CO]$. [f] Tricarbonyl CO species on Ru^{n+}, $[Ru^{n+}(CO)_3, n = 1-3]$. [g] Resolved into three bands at 2045, 2059, and 2074 cm^{-1} (absolute peak area: 0.27, 0.25, and 0.14, respectively).

additional band at 2132 cm^{-1}, which becomes discernible only at temperatures above 150 °C. Similar to what was observed with Ru/Al_2O_3, the band at 2146 cm^{-1} appears to be more sensitive to temperature than the band at 2132 cm^{-1}. The positions of both bands are once again independent of surface coverage. Finally, the enlargement of the HF_1 region also reveals that as the surface coverage decreased to a great extent at 300 °C (trace vii), three bands became apparent at 2073, 2058, and 2045 cm^{-1}. These bands are strongly overlapped at higher surface coverages and hence, not observable at lower temperatures. Additionally, the positions of these bands are likely to have been red-shifted as the temperature increased because of the decrease in surface coverage that led to a weaker dipole−dipole coupling. Hence, it is likely that these bands are originally located in the 2060−2085 cm^{-1} region at room temperature.

On the basis of the results discussed above, the spectra of Figure 3 have been fitted using 10 bands, as shown in Figure 4, with the corresponding band positions and absolute and relative areas summarized in Table 2. Although the feature in the 2060−2085 cm^{-1} region consists of up to three independent bands at close proximity, only a single band was used during the fitting for simplicity (Table 2, band 7). The results of Table 2 show that the bands observed on Ru/SiO_2 are very similar to those observed on Ru/Al_2O_3 with only slight differences in band frequencies and relative intensities. The only exception is the strong band at 2015 cm^{-1} observed on Ru/Al_2O_3 (Table 1, band 4), which is absent from the spectra of Ru/SiO_2.

3.1.2. Sintered Ru/Al_2O_3 Sample. For comparison purposes, similar experiments were also performed on a Ru/Al_2O_3 sample that was first treated in O_2 followed by a subsequent reduction in H_2 (Figure 5). The spectra obtained are similar to those obtained from the samples that only underwent reduction in H_2, with small differences observed in peak positions and relative intensities. However, the absolute intensities of the spectra obtained were substantially lower because of the severe sintering of the sample following the oxidation treatment, as has been reported previously in the literature.[20,23−26] As a result of this sintering, the number of available surface Ru adsorption sites is decreased substantially, resulting in a decrease in the number of adsorbed CO molecules, and hence, in spectral intensity, with the total spectral area reduced by 60%. The spectra were fitted

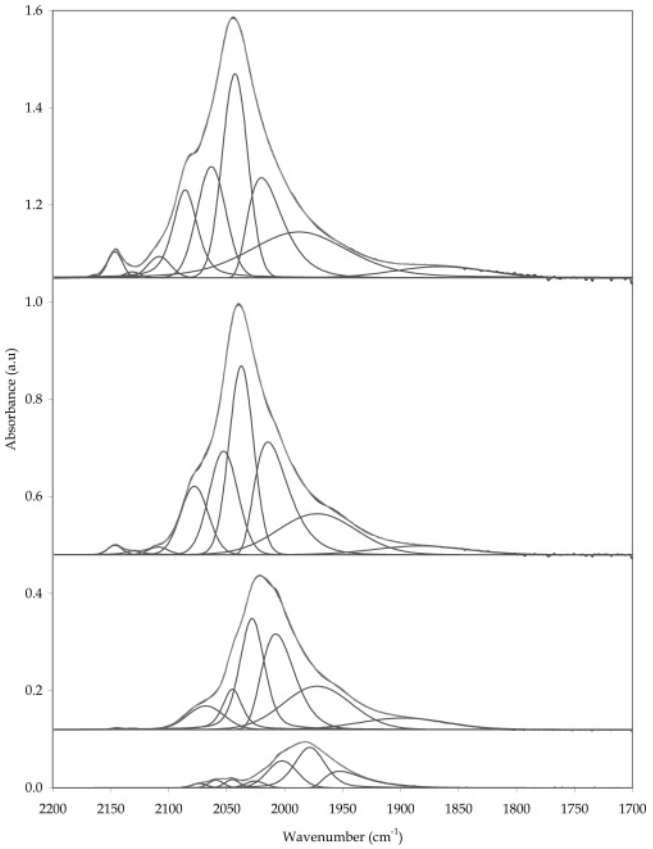

Figure 4. Fitting of selected spectra (i.e., from top to bottom, i, iii, v, and vi) from Figure 3.

using the same set of bands described in detail in the previous section. The band positions and absolute and relative areas obtained are summarized in Table 3. The results indicate that all bands observed previously were also observed in this case.

3.2. CO Adsorption at Elevated Temperatures. A. Ru/Al_2O_3. Spectra of Ru/Al_2O_3 (pretreated in H_2 at 300 °C) collected at various temperatures up to 300 °C in the presence of 1% CO are shown in Figure 6. The spectra were fitted using the same set of peaks used to fit the spectra of Figure 1, and the results

TABLE 3: Characteristic Frequencies and Peak Areas of Spectral Features Observed Following the Room Temperature Adsorption of CO on Ru/Al_2O_3 (Pretreated in O_2 at 300 °C Followed by H_2 at 300 °C) and Subsequent Desorption in He at Different Temperatures

	Ru/Al_2O_3[a]										
temperature/band (°C)	1	2	3	4	5	6	7	8	9	10	11
25	1777	1961	1990	2019	2042	2063	2081	2106	2128	2142	2156
absolute area (au)	0.54	5.51	4.99	5.47	5.62	5.64	2.06	0.42	0.25	0.31	0.03
relative area (%)	1.7	17.9	16.2	17.8	18.2	18.3	6.7	1.4	0.8	1.0	0.1
300	1795	1941	1967	1998		2047					
absolute area (au)	1.29	3.93	5.59	4.12		7.91					
relative area (%)	5.0	17.3	24.6	18.2		34.9					

[a] Refer to Table 1 for band assignments.

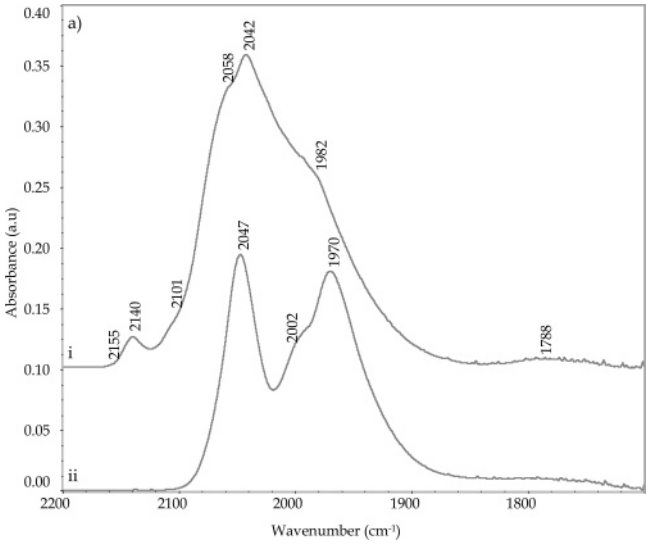

Figure 5. FTIR spectra collected following adsorption of CO at room temperature on Ru/Al_2O_3 pretreated in O_2 at 300 °C followed by a subsequent reduction step in H_2 at 300 °C; (i) 25 and (ii) 300 °C.

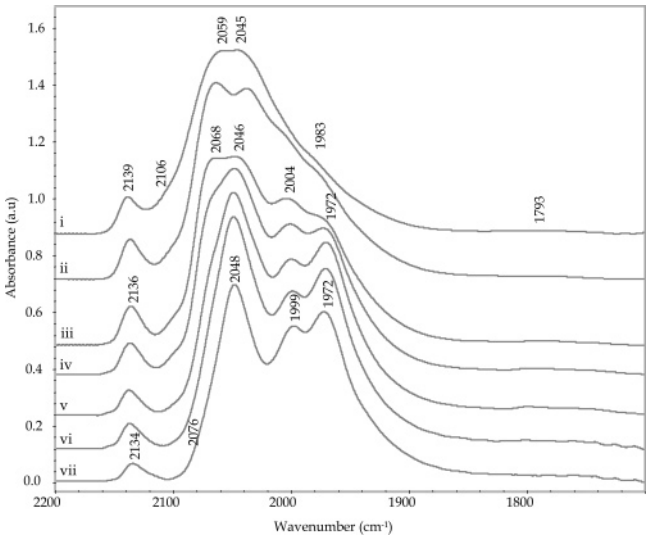

Figure 6. FTIR spectra of Ru/Al_2O_3 (pretreated at 300 °C in H_2) collected in the presence of 1% CO in He at (i) 25, (ii) 70, (iii) 110, (iv) 150, (v) 210, (vi) 250, and (vii) 300 °C.

are summarized in Table 4. The spectrum obtained at room temperature is very similar to the one shown in Figure 1, collected following He flushing at the same temperature. However, substantial differences were observed at elevated temperatures between spectra collected in the presence of CO (Figure 6) and spectra collected during desorption of CO (Figure 1). More specifically, in the former case as the temperature

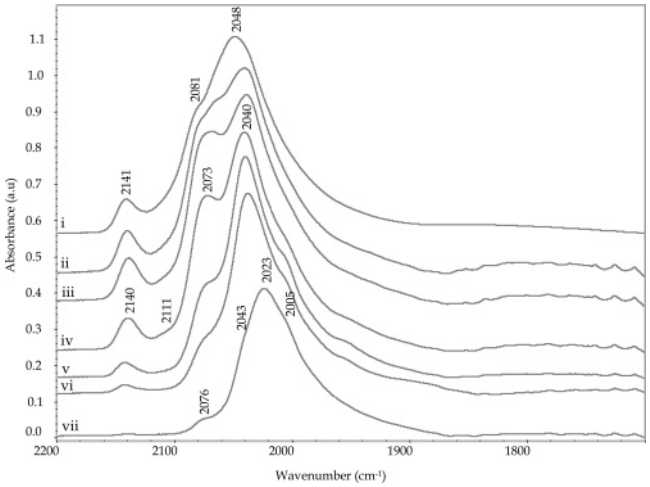

Figure 7. FTIR spectra of Ru/SiO_2 (pretreated at 300 °C in H_2) collected in the presence of 1% CO in He at (i) 25, (ii) 70, (iii) 110, (iv) 150, (v) 210, (vi) 250, and (vii) 300 °C.

increased the intensity of the bands in the 2060−2080 and 1970−2000 cm^{-1} regions increase, yielding at 110 °C a broad unresolved band in the 2040−2080 cm^{-1} range as well as new bands at 2004 and 1972 cm^{-1}. Further increase of the temperature results in a significant decrease in the intensity of the higher frequency side of the broad band in the 2060−2080 cm^{-1} region, resolving a strong symmetric peak centered at 2048 cm^{-1}. Consequently, at higher temperatures, the spectra become similar to the ones obtained during the desorption experiments, but with a higher intensity. Furthermore, most adsorbed species remained on the surface at higher temperatures in the presence of gas-phase CO. For example, the intensities of the peaks at 2134, 2048, 1999, and 1972 cm^{-1} at 300 °C are substantially higher in the spectra of Figure 6 than the spectra of Figure 1.

B. Ru/SiO_2. Spectra of Ru/SiO_2 (pretreated in H_2 at 300 °C) collected at various temperatures up to 300 °C in the presence of 1% CO are shown in Figure 7. The spectra were fitted using the same set of peaks used to fit the spectra of Figure 3, and the results are summarized in Table 5. Once again, the results are similar to those obtained during the desorption of CO (Figure 3). Furthermore, an increase in intensity of the 2060−2080 cm^{-1} region is observed with increasing temperature (as with Ru/Al_2O_3), revealing the presence of more than one band in this region. However, unlike what was observed with Ru/Al_2O_3, the intensities of these features decrease rapidly with further increase in temperature, leaving at 300 °C only a weak shoulder at 2076 cm^{-1} and a band at 2023 cm^{-1} with shoulders at 2005 and 2043 cm^{-1}. Additionally, the band in the HF_1 region disappeared completely at 250 °C, a temperature that is lower than the one observed on Ru/Al_2O_3 (above 300 °C), consistent with the results of the desorption experiments (Figures 1 and 3).

TABLE 4: Characteristic Frequencies and Peak Areas of Spectral Features Observed in Spectra of Ru/Al_2O_3 (Pretreated in H_2 at 300 °C) Collected at Different Temperatures in the Presence of 1% CO[a]

temperature/band (°C)	1	2	3	4	5	6	7	8	9	10	11
25	1792	1959	1989	2014	2038	2061	2080	2105	2130	2141	2155
absolute area (au)	0.89	8.08	9.81	9.49	16.91	12.72	10.72	17.48	1.56	1.4	0.08
relative area (%)	1.0	9.1	11.0	10.6	19.0	14.3	12.0	19.6	1.1	1.6	0.1
110	1782	1953	1978	2004	2033	2055	2074	2100	2131	2139	2153
absolute area (au)	2.54	13.03	13.83	13.5	15.07	15.52	10.63	1.79	1.88	1.04	0.12
relative area (%)	2.9	14.7	15.6	15.2	16.9	17.4	11.9	2.0	2.1	1.2	0.1
210	1788	1946	1972	2002	2028	2050	2072	2093	2131	2140	2151
absolute area (au)	3.07	12.97	21.94	13.36	10.46	23.60	6.8	0.70	0.85	0.73	0.13
relative area (%)	3.2	13.7	23.2	14.1	11.1	24.9	7.2	0.7	0.9	0.8	0.1
300	1788	1945	1972	2000	2024	2049	2072		2126	2036	2150
absolute area (au)	2.55	13.99	19.54	12.68	8.67	21.41	3.43		0.66	0.63	0.04
relative area (%)	3.0	16.7	23.4	15.2	10.4	25.6	4.1		0.8	0.8	0.0

[a] Refer to Table 1 for band assignments.

TABLE 5: Characteristic Frequencies and Peak Areas of Spectral Features Observed in Spectra of Ru/SiO_2 (Pretreated in H_2 at 300 °C) Collected at Different Temperatures in the Presence of 1% CO[a]

temperature/band (°C)	1	2	3	4	5	6	7	8	9	10	11
25	1831	1973	2015		2042	2063	2084	2106	2131	2143	
absolute area (au)	3.06	8.38	9.55		13.95	8.74	7.24	1.84	1.07	1.21	
relative area (%)	5.6	15.2	17.4		25.4	15.9	13.2	3.3	1.9	2.2	
110	1773	1961	2012		2037	2060	2080	2107	2132	2141	
absolute area (au)	2.50	6.38	11.19		13.32	10.88	9.69	1.01	1.15	1.67	
relative area (%)	4.3	11.0	19.4		23.1	18.8	16.8	1.8	2.0	2.9	
210	1772	1960	2010		2036	2048	2074		2130	2142	
absolute area (au)	0.98	7.48	11.4		13.13	6.71	6.96		0.74	0.49	
relative area (%)	2.0	15.6	23.8		27.4	14.0	14.5		1.5	1.0	
300		1954	1997		2023	2043	2070			2040	
absolute area (au)		4.33	7.18		12.24	3.6	1.33			0.09	
relative area (%)		15.0	25.0		42.6	12.5	4.6			0.3	

[a] Refer to Table 2 for band assignments.

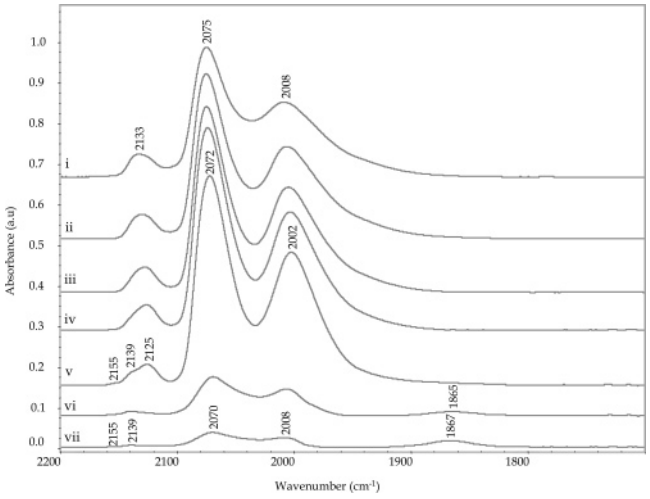

Figure 8. FTIR spectra of Ru/Al_2O_3 (pretreated at 300 °C in H_2) collected in 0.5% CO−0.5% O_2 in He at (i) 25, (ii) 70, (iii) 110, (iv) 150, (v) 210, (vi) 250, and (vii) 270 °C.

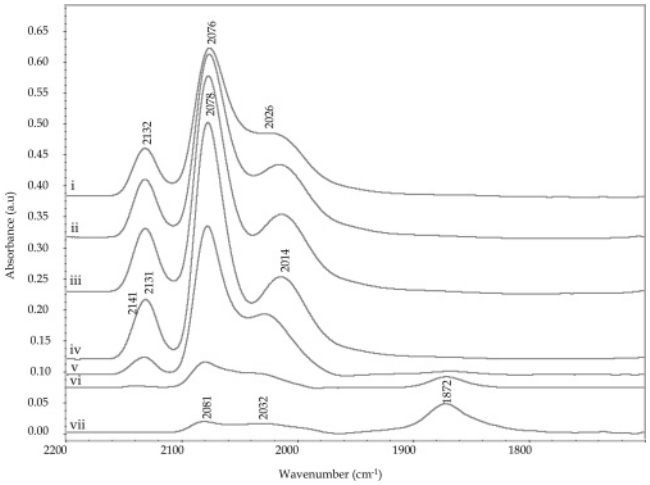

Figure 9. FTIR spectra of Ru/SiO_2 (pretreated at 300 °C in H_2) collected in 0.5% CO−0.5% O_2 in He at (i) 25, (ii) 70, (iii) 110, (iv) 150, (v) 210, (vi) 250, and (vii) 270 °C.

3.3. CO Adsorption at Elevated Temperatures in the Presence of O_2. A. Ru/Al_2O_3. Substantial differences were observed when the same experiments were conducted in the presence of O_2. Three main features were observed at 2133, 2075, and 2008 cm^{-1} at room temperature (Figure 8). At higher temperatures, the band in the HF_1 region downshifted slightly to 2127 cm^{-1} without a significant change in intensity before it resolved into two bands at 2139 and 2125 cm^{-1} at 210 °C. In contrast, the intensities of the bands at 2075 and 2008 cm^{-1} increased with increasing temperature, reaching a maximum at 210 °C before they eventually decreased substantially at 250 °C (trace vi). Additionally, both features at 2075 and 2008 cm^{-1} are observed to downshift slightly. Finally, the intensity of the broad band centered at approximately 1860 cm^{-1} increased slightly at temperatures above 250 °C, in contrast to all other bands in the spectrum.

B. Ru/SiO_2. Similarly, three main features were also observed at room temperature in the spectra of Ru/SiO_2 (Figure 9) at 2132, 2076, and 2026 cm^{-1}. In this case, no apparent shift of the HF_1 band was observed with increasing temperature, although an increase in intensity was observed at temperatures below 110 °C. Above this temperature, the intensity of this band

TABLE 6: Characteristic Frequencies and Peak Areas of Spectral Features Observed in Spectra of Ru/SiO_2 and Ru/Al_2O_3 (Pretreated in H_2 at 300 °C) Collected at Different Temperatures in the Presence of 0.5% CO−0.5% O_2 in He

Ru/Al_2O_3[a]											
temperature/band (°C)	1	2	3	4	5	6	7	8	9	10	11
25		1940	1990	2014	2040	2061	2078	2106	2126	2138	
absolute area (au)		1.64	5.60	4.70	3.89	3.28	6.69	0.23	0.98	0.48	
relative area (%)		6.0	20.4	17.1	14.2	11.9	24.3	0.8	3.5	1.7	
210		1930	1978	2003	2029	2053	2074	2111	2126	2141	2152
absolute area (au)		1.35	4.57	10.21	2.79	5.64	12.55	0.00	1.16	0.17	0.05
relative area (%)		3.5	11.9	26.5	7.2	14.7	32.6	0.0	3.0	0.4	0.1
Ru/SiO_2[a]											
25	1884	1980	2010		2038	2060	2078	2110	2128	2138	
absolute area (au)	0.26	1.61	2.86		3.2	1.93	6.42	0.19	1.30	0.70	
relative area (%)	1.4	8.7	15.5		17.3	10.5	34.7	1.1	7.0	3.8	
150		1950	2007		2031	2058	2078		2129	2138	
absolute area (au)		0.36	4.63		2.79	2.85	9.62		2.04	0.48	
relative area (%)		1.6	20.4		12.2	12.5	42.3		9.0	0.7	

[a] Refer to Tables 1 and 2 for band assignments.

decreased substantially and it disappeared at 250 °C. The intensities of the bands at 2076 and 2026 cm^{-1} also increase with increasing temperature, with the bigger increase observed at 2076 cm^{-1}. A maximum was observed at 150 °C and a rapid decrease in intensity followed at higher temperatures. Furthermore, the band at 2026 cm^{-1} shifted to 2014 cm^{-1} at 150 °C, and back to 2027 cm^{-1} at higher temperatures, suggesting substantial changes in the relative intensities of the different peaks in this region. Once again, further increase in temperature above 210 °C resulted in an increase in intensity of the broad band at 1872 cm^{-1}, although in this case, the increase was more pronounced than that observed on Ru/Al_2O_3. Examples of fitting results, obtained using the same sets of peaks as before, are presented in Table 6.

It appears that even the presence of small amounts of oxygen can result in substantial differences in the spectra obtained. In fact, the presence of trace amounts of oxygen may have affected spectra reported earlier and collected under otherwise "reducing" conditions,[20] although the quantitative conclusions drawn in this earlier publication regarding the strength of adsorption of CO are unaffected.

4. Discussion

4.1. Band Assignments. A. Ru/Al_2O_3. The fitting results summarized in Table 1 show that the adsorption of CO on Ru/Al_2O_3 at room temperature gives rise to a total of 11 bands in the IR spectra: at 1789, 1959, 1990, 2015, and 2038 cm^{-1} in the LF region; at 2062, 2080, and 2107 cm^{-1} in the HF_2 region; and at 2130, 2141, and 2154 cm^{-1} in the HF_1 region. Most of these bands have also been observed previously as indicated in the literature, although the assignments of some of them remain under debate. There is, however, a general agreement on the band observed at approximately 2040 cm^{-1}, which has universally been assigned to linearly bonded CO on zerovalent Ru sites.[4,30] On single crystals of Ru(001), the position of this band has been reported to shift from 1984 to 2060 cm^{-1} as the CO coverage increases from 0.003 to 0.66.[27,28] The room-temperature spectra of supported reduced Ru samples containing large particles are typically dominated by this band centered at 2040−2060 cm^{-1}.[6,8,29] Furthermore, the corresponding linearly bonded CO species exhibits moderate stability, and remains mostly intact upon evacuation at room temperature. Nevertheless, its concentration, and consequently, the intensity of the 2040 cm^{-1} band decreases rapidly with increasing evacuation temperature.[5,8,19,30] In the present study, this band decreased in intensity and shifted from 2038 cm^{-1} at room temperature to 2025 cm^{-1} at 210 °C, presumably because of the decreasing coverage and hence the reduced CO coupling effect. Above this temperature it became poorly resolved and disappeared (Figure 1).

It has been observed previously that upon room-temperature adsorption of CO on Ru bands in the 2070−2080 cm^{-1} region develop in parallel with bands in the HF_1 region (i.e., 2130 and 2140 cm^{-1}). Such pairs have been assigned to the asymmetric and symmetric stretching, respectively, of multicarbonyl species on partially oxidized Ru sites, (i.e., $Ru^{n+}(CO)_x$), although there is no universal agreement regarding the oxidation state of Ru (n) and the number of carbonyl groups (x). Several studies on various supported Ru catalysts have reported that the HF_1 band is centered at approximately 2140 cm^{-1},[7,8,9] while others have observed it at approximately 2130 cm^{-1}.[31] It is possible that both bands are present in all cases, but because of differences in the relative intensities, only one is observed if no fitting of the spectra is attempted. In the present study, the band at 2140 cm^{-1} is dominating the region and is the only one clearly visible at room temperature (Figure 1). Nevertheless, deconvolution of the spectra along with the results obtained at higher temperatures clearly indicate the presence of the second band at 2130 cm^{-1} as well. We can therefore conclude that there are at least two different adsorbed species, possibly with similar structures and on similar adsorption sites, giving rise to two pairs of IR bands in the HF_1 and HF_2 regions. This is further illustrated by the data of Table 1 and Figure 10, which show that the intensities of the two bands at 2130 and 2141 cm^{-1} (bands 9 and 10, respectively) decrease in parallel with the intensity of the band at 2080 cm^{-1} (band 7) with increasing temperature.

A number of different studies have assigned bands at 2145−2125 and 2080 cm^{-1} to a tricarbonyl CO species adsorbed on Ru^{n+} based on results obtained using $^{12}CO-^{13}CO$ isotopic mixtures.[2,7,9,17] Others have argued that the number of carbonyl groups may actually be between 3 and 4 (based on comparisons of the band frequencies observed with those of known Ru carbonyl complexes[10]) or even 2 (also based on results obtained from isotopic exchange experiments[11,15]). In all of these studies, the conclusions were drawn based on the number of bands observed in the HF_1 region during $^{12}CO-^{13}CO$ isotopic exchange experiments because the bands in the HF_2 and LF regions are heavily overlapped.

Although no definite conclusion can be drawn from the results of the current study regarding the type of species that gives

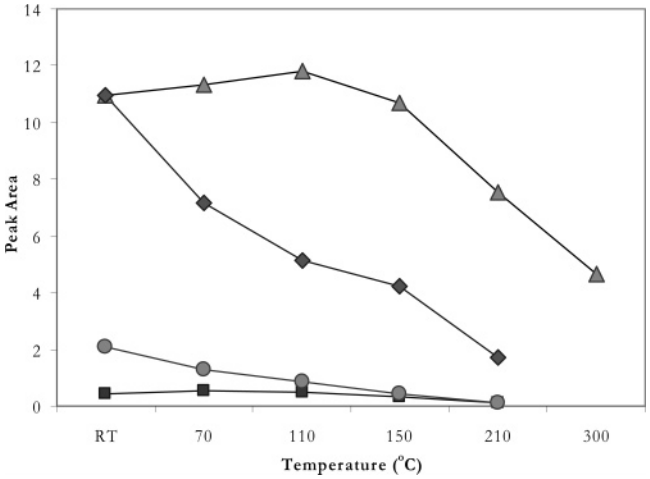

Figure 10. Absolute peak areas of bands 4 (▲), 7 (◆), 9 (■), and 10 (●) of Table 1, as functions of temperature.

rise to this pair of bands and, more specifically, the number of carbonyl groups involved, a careful review of the literature has led us to believe that a tricarbonyl species is formed. Previous studies that concluded the presence of such a species were conducted using a series of varying concentrations of ^{12}CO and ^{13}CO, and, hence, were able to discern peaks that would otherwise be overlapped by stronger neighboring bands.[7,9,17] In contrast, studies that concluded the presence of a dicarbonyl species were performed using only a single concentration of a $^{12}CO-^{13}CO$ mixture and the poorly resolved spectra obtained may have led to false conclusions.[11,15] Furthermore, the positions of the bands are very similar to those observed for ruthenium tricarbonyl complexes having a stoichiometry $Ru_2(CO)_6X_4$ (where X is Cl, Br, or I), which exhibit strong absorbances at 2143−2128 and 2075−2069 cm^{-1} and a weak absorbance at 2015−2010 cm^{-1}.[10,32,33] The exact positions of these bands are dependent on the electronegativity of the halogen ligands, with a downshift observed with decreasing electronegativity.[32,33] In the case of supported Ru catalysts, the formation of the tricarbonyl species is believed to be the result of a CO-induced oxidative disruption process of finely dispersed Ru clusters with the participation of hydroxyl groups from the support, forming electron-deficient Ru^{n+} (n ranging between 1 and 3) sites with Y−O−Ru linkages (Y = Al, Si, or Ti).[7,9,13]

On the basis of the above, the two bands observed in our study at 2130 and 2140 cm^{-1} can be assigned to the symmetric stretching vibrations of two tricarbonyl species adsorbed on Ru^{n+}, with slightly different properties. Previous studies have reported that the adsorption of CO on a Ru surface preexposed to O_2 at room temperature produces HF bands at 2130 and 2070 cm^{-1} [5,8,16] as opposed to 2140 and 2080 cm^{-1} on a sample that had undergone a H_2 treatment. Hence, it is likely that the species that gives rise to the band at 2130 cm^{-1} in our case is perturbed by neighboring O atoms to a higher degree. This is also consistent with the results obtained in the presence of O_2 (Figures 8 and 9), which indicate that in that case the band at 2130 cm^{-1} dominates the one at 2140 cm^{-1}, resulting in a single apparent band in the unresolved spectrum at a frequency close to 2130 cm^{-1}. Yet, the presence of a band representing CO adsorption on a more oxidized surface at a lower wavenumber appears somewhat odd. Yokomizo et al.[7] have proposed that such an observation can be rationalized if the band at 2130 cm^{-1} is due to a tricarbonyl species adsorbed on $Ru^{\delta+}$ ions present on the oxidized surface of Ru particles, (i.e., $(RuO)_xRu^{n+}(CO)_3$ type species). In such a structure, the Ru atom attached to the CO ligand is more electron-dense than a similar Ru atom residing on the oxide support (i.e., in an $(AlO)_xRu^{n+}(CO)_3$ type species). Therefore, such a species can give rise to absorbance bands at lower wavenumbers. The presence of both bands at 2130 and 2140 cm^{-1} in our spectra suggests that both types of structures are formed on the Ru samples, although a higher concentration of the $(AlO)_xRu^{n+}(CO)_3$ type species is suggested by the higher intensity of the 2140 cm^{-1} band. The positions of both bands do not shift with coverage (Figure 1 and Table 1), consistent with an assignment to isolated Ru atoms bonded directly to the support or RuO. Although our curve-fitting results (Table 1) indicate that the HF_2 component of these same species shifts by approximately 4 cm^{-1} between room temperature and 210 °C (from 2080 to 2076 cm^{-1}), such a difference is definitely within the margin of error of our experimental measurements and the subsequent analysis. Furthermore, several studies have reported a faster rate of growth of the 2080 cm^{-1} band upon CO adsorption relative to the rate of growth of the corresponding bands in the HF_2 region, suggesting the existence of another adsorbed species with a similar stretching frequency, most likely, linearly adsorbed CO on $Ru^{\delta+}$ sites.[5,7]

The HF_2 region is further complicated by the presence of an additional band assigned to a dicarbonyl species (type III carbonyl). The symmetric and asymmetric stretching vibrations of such a species give rise to a pair of bands in the HF_2 (2070−2080 cm^{-1}) and LF (2010 ± 10 cm^{-1}) regions.[15,18] Hence, the HF_2 band at the 2070−2080 cm^{-1} region also contains a contribution from this species. Two bands at 2015 and 2080 cm^{-1} similar to the ones observed in the current study (bands 4 and 7, respectively) were observed previously as "shoulders" and were assigned to a dicarbonyl species adsorbed on Ru^{2+}.[15] The intensities of these two bands are observed to decrease in parallel with increasing temperature (Figure 10). Our fitting results (Table 1) indicate that the LF component of this species (band 4) experiences a red shift on the order of 15 cm^{-1} with temperature. Once again, we cannot exclude the possibility that an additional surface species may also be contributing to the intensity of this band. For example, a band at approximately 2010 cm^{-1} is frequently assigned to linearly adsorbed CO on higher energy Ru defect sites and/or isolated Ru^0 sites surrounded by partially oxidized Ru^{n+} sites. Such sites, because of either a stronger back-donation of d electrons from the metal into the π^* orbitals of CO or a weaker dipole coupling interaction, can lead to the appearance of a new band or substantial tailing in the lower frequency region of the more prominent 2040 cm^{-1} band discussed above.[34] In fact, our results are slightly different from those reported by Zecchina et al., who observed the parallel growth and disappearance of a pair of bands at 2075 and 2005 cm^{-1}.[14] As can be seen in Figure 1, at 300 °C, when the band at 2070−2080 cm^{-1} has already disappeared completely, the band at 2000 cm^{-1} can still be observed as a well defined shoulder, which is consistent with other previous reports,[21,35] suggesting that a percentage of band 4 in the 2000−2015 cm^{-1} region is due to contributions from a monocarbonyl species adsorbed on isolated Ru^{n+} sites.

The fitting results further suggest the presence of an additional dicarbonyl species, giving rise to a pair of bands in the HF_2 and LF regions, at frequencies approximately 20−30 cm^{-1} lower at room temperature than those of the dicarbonyl species described previously (i.e., 2062 and 1990 cm^{-1}; bands 6 and 3).[14,15] These bands are very stable and remained in the spectra at temperatures up to at least 300 °C (Figure 1 and Table 1). Similar to the tricarbonyl species described above, the band positions are comparable to those observed for Ru dicarbonyl

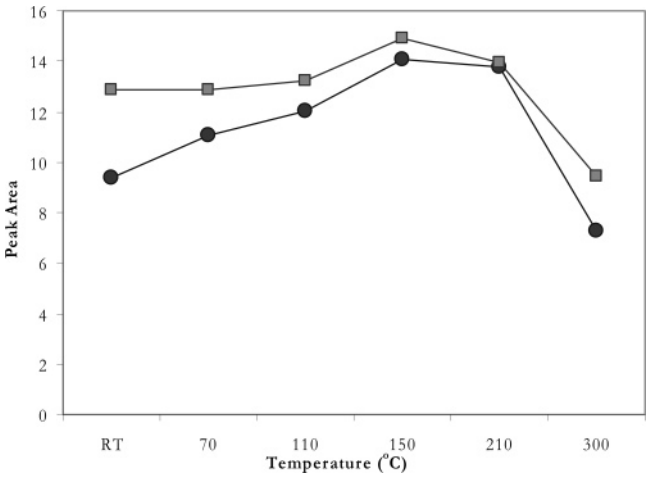

Figure 11. Absolute peak areas of bands 3 (●) and 6 (■) of Table 1, as functions of temperature.

complexes having a $Ru(CO)_2X_2$ stoichiometry (where X is Cl, Br, or I), which appear at 2066−2053 and 1995−1988 cm^{-1}.[10,33] On the basis of the same reasoning as above, and the results of $^{12}CO-^{13}CO$ isotopic substitution experiments that yielded a total of six bands, these bands were previously assigned to a dicarbonyl species adsorbed on Ru^{n+}, where *n* is suggested to be equal to 2 for the species giving rise to the pair of bands at higher frequencies (i.e., 2080 and 2015 cm^{-1}) and 0 for the species giving rise to the pair of bands at lower frequencies (i.e., 2062 and 1990 cm^{-1}).[14,15] The latter pair of bands experiences a gradual red shift of approximately 10 cm^{-1}, with decreasing surface coverage up to approximately 210 °C, suggesting that the corresponding species are not isolated. At temperatures above 150 °C, the shift becomes minimal because of a limited dipole−dipole coupling interaction at low surface coverages. It is thus possible that this dicarbonyl species is present on the surface as patches or islands separated from one another. The intensities of these bands increased gradually with temperature up to approximately 200 °C, and then decreased rapidly at higher temperatures (Figure 11). Such a behavior may suggest an interconversion between different species as the surface coverage changes. For example, it is possible that as the linear CO species desorb from the densely populated Ru^0 sites, the freed up sites allow the remaining adsorbed CO species to rearrange into the more stable dicarbonyl species, which persists up to 300 °C.

A low intensity band observed at frequencies below 1800 cm^{-1} (band 1) can be assigned to bridge-bonded CO on metallic Ru.[21,36] This band accounts at most for 5.0% of the total spectral area. Its intensity remained relatively constant up to 150 °C, and then increased slightly at 210 °C, presumably because of a decrease in the total surface coverage that allows a conversion of a small fraction of the linearly-bonded CO molecules to bridged ones before desorption at even higher temperatures. A similar conversion of linearly-bonded to bridged CO species during the thermal desorption of CO has also been observed with Rh/TiO_2 catalysts.[37]

The two bands observed at 1950 and 2110 cm^{-1} (bands 2 and 8) have also been observed in previous studies of CO adsorption on supported Ru catalysts,[2,16,31] although their origin has not been investigated extensively. These bands usually appear as weak shoulders on the much stronger neighboring bands, and thus, have been often overlooked. It has been suggested that the band at 1950 cm^{-1} can be assigned to a bridge-bonded CO on Ru^0 species with a slightly different energy than the similar species appearing at lower wavenumbers.[16,31,38] According to our fitting results (Table 1) the intensity of this band increases slightly with increasing temperature up to approximately 150−200 °C, above which it decreased rapidly. Once again, this behavior could be attributed to the decrease in total surface coverage, which allows the formation of new bridged sites and the conversion of some linearly to bridged-bonded molecules prior to desorption.

Finally, following previous literature report the band at approximately 2110 cm^{-1} (band 8) can be tentatively assigned to linearly adsorbed CO on oxidized Ru^{n+} sites.[2] Because this band disappeared completely at temperatures above 110 °C, such a species is relatively unstable. Similarly, a weak feature observed in the HF_1 region at 2155 cm^{-1} (band 11) has been assigned to a similar linearly adsorbed CO species on Ru^{n+} sites, which have been oxidized to a greater extent.[4]

B. Ru/SiO_2. Similar to Ru/Al_2O_3, the band observed at 2043 cm^{-1} (band 5) at room temperature on Ru/SiO_2 can be assigned to linearly adsorbed CO on Ru^0. In contrast to Ru/Al_2O_3, however, this band remained visible in the Ru/SiO_2 spectra at temperatures up to 300 °C, although with much lower intensity and a downshifted frequency. This result suggests a stronger bonding of linearly adsorbed CO on Ru/SiO_2 than on Ru/Al_2O_3, although the total CO adsorption is less stable as discussed later. However, it is possible that the linear species also remained adsorbed on Ru/Al_2O_3 at 300 °C, with a small band intensity, hence, being obscured by the much stronger neighboring bands.

Similarly, bands in the HF_1 region, at 2146 and 2132 cm^{-1} (bands 9 and 10), together with bands in the 2060−2086 cm^{-1} region can be assigned to a tricarbonyl species adsorbed on partially oxidized Ru^{n+}. Once again the band at 2060−2086 cm^{-1} (band 7) includes contributions from several different species, some of which become discernible only at very low surface coverages (i.e., at 300 °C) as shown in Figure 3. These species, as discussed above for Ru/Al_2O_3, include at least two different forms of tricarbonyls and a monocarbonyl species on partially oxidized Ru^{n+}. The dicarbonyl species observed on Ru/Al_2O_3 is absent in this case because the asymmetric 2000−2015 cm^{-1} band (band 4) is not present in the LF region (Table 2). Furthermore, the two bands assigned to the tricarbonyl species in the HF_1 region at 2146 and 2132 cm^{-1} have disappeared completely at 300 °C, and, hence, the bands remaining in the HF_2 region cannot be attributed to the tricarbonyl species. Nevertheless one of the bands observed in the 2060−2086 cm^{-1} region can be assigned to the linear monocarbonyl species on oxidized Ru^{n+} sites. It is possible that the remaining two bands represent monocarbonyl species formed during the partial desorption of CO from the tricarbonyl adsorption sites. If this is indeed true, then two of the bands in this region should not shift with surface coverage because they arise from species adsorbed on isolated Ru sites attached to either the support or RuO, as described previously. Only a small blue-shift may be observed during the conversion of the tricarbonyl to monocarbonyl species because of small changes in the distribution of electron density in Ru. Therefore, the overall shift of the main composite band from 2086 to 2068 cm^{-1} may be attributed primarily to the coverage effects associated with the linearly adsorbed monocarbonyl species. The existence of these three bands was not observed on Ru/Al_2O_3 even at high temperatures because they most likely were completely overlapped by the strong remaining band centered at 2049 cm^{-1}.

The most important difference between Al_2O_3- and SiO_2-supported Ru, however, is the absence of the dicarbonyl species on Ru^{2+} (bands 4 and 7) on Ru/SiO_2. It is likely that the surface

TABLE 7: Relative Ratios of Band Intensities Observed in the Room Temperature Spectra of Finely Dispersed (i.e., H_2 Treatment) and Sintered (i.e., O_2-H_2 Treatment) Ru/Al_2O_3 Samples

Ru/Al_2O_3		
	pretreatment conditions	
relative band intensities	H_2	O_2-H_2
band 5/band 4	1.3	1.0
band 5/band 3	1.5	1.1
band 5/band 10	6.9	18.1
band 10/band 9	4.7	1.2

of Ru supported on SiO_2 is reduced to a greater extent than the surface of Ru supported on Al_2O_3 following reduction at 300 °C because of a stronger metal support interaction and a smaller particle size in the case of Al_2O_3.[20] As a result, Ru particles on Al_2O_3 may remain more electron-deficient. In fact, it has been reported previously that SiO_2-supported Ru is reduced completely,[39,40] while Al_2O_3-supported Ru remains partially oxidized[21] following H_2 treatment. Consequently, the absence of oxidized Ru^{2+} sites in the Ru/SiO_2 sample can explain the absence of the dicarbonyl species giving rise to bands 4 and 7. Nevertheless, our results suggest that a small number of Ru^{n+} sites are present on Ru/SiO_2, some of which are located in isolated small Ru clusters that allow the formation of a tricarbonyl species via oxidative disruption.

In the case of Ru/SiO_2, a dicarbonyl species is also formed on Ru^0 (bands 3 and 6). These two dicarbonyl bands appear at 2020 and 2063 cm^{-1} at room temperature and eventually are red-shifted to 2008 and 2045 cm^{-1} at 210 °C. Once again, the fitting results for the LF component of this species (band 3) may be affected to a large extent by CO adsorption on higher energy defects sites or isolated Ru^0 sites surrounded by partially oxidized Ru^{n+} sites. This contributes to the tailing at the lower frequency side of the linear band at 2043 cm^{-1} (band 5). This becomes evident at higher temperatures (i.e., above 200 °C), where the intensity of band 6 decreases more rapidly than that of band 3. For example, at 300 °C the ratio of the intensities of bands 3 and 6 is on the order of 10, strongly suggesting the presence of an additional species with absorbance in the LF region. We should finally point out that because of the nature of CO adsorption on Ru/SiO_2 (i.e., bands remaining convoluted in the LF region even at higher temperatures), the position of these bands reported in Table 2 may contain a greater error than the corresponding results shown in Table 1 for Ru/Al_2O_3.

Finally, the two bands observed at 2111 and 2165 cm^{-1} (bands 8 and 11) can be assigned to linearly adsorbed CO on partially oxidized Ru^{n+} sites, with n being greater for the species giving rise to the band at 2165 cm^{-1}. It is interesting to note that the band at 2165 cm^{-1} appears only at room temperature (Figure 3), suggesting that the adsorption of this species is weaker on Ru/SiO_2 than on Ru/Al_2O_3. In contrast, the species giving rise to the band at 2110 cm^{-1} appears to have similar stability on both samples, desorbing completely at temperatures above 110 °C.

The above results including band frequencies, adsorption sites, and the main characteristics of the various adsorbed CO species on supported Ru catalysts are summarized in Table 8.

4.2. CO Adsorption on Severely Sintered Ru/Al_2O_3. In the spectra of the sintered Ru/Al_2O_3 sample (i.e., the sample that underwent O_2 treatment prior to reduction), the relative ratios of the different bands vary from what was observed previously with the finely dispersed samples (Table 7). In general, the ratios of the intensity of band 5 (linearly adsorbed CO) to the intensities of bands in the lower frequency region have decreased, whereas the ratios of the intensity of band 5 to those of bands in the higher frequency region have increased. One possibility is that the reduction of Ru in this case has been incomplete because of the prior oxidation step. This would increase the relative amount of linearly adsorbed CO on Ru^0 surrounded by partially oxidized sites (band 4), as opposed to CO adsorbed on metallic Ru^0 sites (band 5), leading to a lower ratio of the two. Conversely, the ratio of linear adsorption (band 5) to that of tricarbonyl adsorption (band 10) increases by a factor of 3. This is not surprising because the sample is severely sintered upon the O_2-H_2 treatment, and hence, tricarbonyl adsorption is hindered because of a lack of isolated sites and/or small clusters, which are necessary for tricarbonyl adsorption to occur via oxidative disruption. Additionally, the relative ratio of the bands at 2140 and 2130 cm^{-1} (band 10/band 9) decreases on the severely sintered sample, suggesting a decrease in the number of isolated sites bonded directly to the support relative to those bonded to RuO. This also indicates the presence of larger Ru particles and a relatively higher amount of RuO on the severely sintered sample because of the prior oxidation treatment.

4.3. Stability of the Adsorbed CO Species. In general, the analogous CO species adsorbed on Ru supported on Al_2O_3 are more stable than those supported on SiO_2. This is indicated clearly by the results presented in Tables 1 and 2. At 300 °C

TABLE 8: Summary of Frequencies and Main Characteristics of Various Adsorbed Species Observed on Highly Dispersed Ru/Al_2O_3 and Ru/SiO_2

adsorbed species	adsorption site	frequency(cm^{-1})	characteristics
bridged [$Ru_2-(CO)$]	Ru^0	1750−1990	Low intensities; some formed during desorption of other species at elevated temperatures.
linear [$Ru-CO$]	Ru^0	2000−2050	Moderate stability, remains intact at room temperature but desorbs rapidly with a red shift at higher temperatures.
	Ru^0	∼2010	Isolated Ru^0-CO surrounded by Ru^{n+}; often appears as tailing in the low-frequency side of the previous linear species.
	$Ru^{\delta+}$	∼2080	Red-shifted with coverage.
	Ru^{n+}	∼ 2110	Moderate stability, desorbs at temperatures above 110 °C.
	Ru^{m+} ($m > n$)	2150−2170	Moderate stability, desorbs quickly with increasing temperature.
dicarbonyl species [$Ru-(CO)_2$]	Ru^0	∼1990, 2060	Highly stable, especially on Ru/Al_2O_3
	Ru^{2+}	2015, ∼2080	Less stable than the previous species on Ru^0; not observed on Ru/SiO_2.
tricarbonyl species [$Ru^{n+}-(CO)_3$]	Ru^{n+} ($n = 1-3$)	∼2080, 2140	Isolated sites, bonded directly to the support, i.e., $[(SiO)_xRu^{n+}(CO)_3]$; does not shift with coverage; present up to 200 °C.
	Ru^{n+} ($n = 1-3$)	∼2070, 2130	Isolated Ru^{n+} sites bonded on RuO particles, i.e., $[(RuO)_xRu^{n+}(CO)_3]$; does not shift with coverage; present up to 200 °C.

for example, the amount of CO remaining on Ru/SiO_2 is reduced to a greater extent than on Ru/Al_2O_3 (i.e., 14% vs 35%, respectively).

On Ru/Al_2O_3, the most stable species appears to be the dicarbonyl species adsorbed on Ru^0 (i.e., $Ru^0-(CO)_2$), which gives rise to bands 3 and 6 (1970−1990 cm^{-1} and 2049−2062 cm^{-1}, respectively). This species remained on the surface at elevated temperatures both in the presence and absence of gas-phase CO (Figures 1 and 6). In fact, at temperatures above 200 °C, the corresponding bands become the dominant features of the spectra, and their intensities remain strong even at 300 °C. Furthermore, the observed increase in the surface concentration of this species with increasing temperature in the presence of gas-phase CO suggests that its formation is favored at high temperatures (Figure 6). In contrast, on Ru/SiO_2, this species is clearly less stable and disappeared rapidly from the surface with increasing temperatures (Figure 3). Similar to Ru/Al_2O_3, in the presence of gas-phase CO its surface concentration also increased with increasing temperature, although a maximum was observed at 150 °C and a substantial decrease was evident at higher temperatures (Figure 7). We can tentatively attribute this behavior to differences in metal−support interactions, which result in the creation of similar adsorption sites on both supports but with different chemisorptive properties. The stronger metal−support interactions in the case of Ru/Al_2O_3 result in the formation of smaller metal particles than those on Ru/SiO_2 upon treatment under the same conditions.[20] These smaller particles are expected to have higher density of defect sites, which may be the reason for the stronger multicarbonyl adsorption on Ru/Al_2O_3.

Similarly, the tricarbonyl species that gives rise to two pairs of bands in the HF_1 and HF_2 regions appears to be more stable on Ru/Al_2O_3 than on Ru/SiO_2. In the absence of gas-phase CO, this species remained adsorbed on Ru/Al_2O_3 at 250 °C, while it is no longer observed on Ru/SiO_2 at the same temperature. The same is true in the presence of gas-phase CO, although in this case the tricarbonyl species remained on both surfaces at even higher temperature. Furthermore, when comparing the two tricarbonyl species at 2140 and 2130 cm^{-1} (bands 10 and 9), on both supports, it is observed that the ratio of the two decreases substantially when gas-phase CO is present (Tables 1 and 2 vs Tables 4 and 5). This suggests that the tricarbonyl species at 2130 cm^{-1} are less stable compared to that at 2140 cm^{-1} and, hence, require a higher CO pressure to remain adsorbed on the surface.

4.4. CO Adsorption in the Presence of O_2. In the presence of O_2, on both the Al_2O_3- and SiO_2-supported Ru samples, the HF_1 band in the deconvoluted spectra appears now to be centered at approximately 2130 cm^{-1} at room temperature, consistent with previous literature reports.[5,8,16] The apparent "red shift" of this feature is the result of a substantial increase in the relative intensity of band 9 to band 10 in the presence of O_2. For example, for Ru/SiO_2 in the presence of O_2, when the ratio of the intensities of band 9 to band 10 is approximately 2, the composite "apparent" peak appears to be centered at approximately 2132 cm^{-1} (Figure 9, trace i). In comparison, in the absence of O_2, when the ratio of the intensities of band 9 to band 10 is less than 1, the composite apparent peak appears to be centered at approximately 2141 cm^{-1} (Figure 7, trace i). These changes are consistent with the assignment of band 9 to tricarbonyl species adsorbed on Ru sites perturbed by O atoms to a greater extent, or on Ru^{n+} sites located on RuO.

On both supports, the band in the 2070−2080 cm^{-1} region now becomes the dominating feature of the spectra, and its intensity increases with increasing temperature up to 200−250 °C. As discussed above, this band includes contributions from two different forms of tricarbonyl, a dicarbonyl, and a monocarbonyl species, all adsorbed on partially oxidized Ru^{n+} sites. On Ru/Al_2O_3, the relatively constant intensities of the bands in the HF_1 region suggest that the change in the 2075 cm^{-1} band with temperature is not due to an increase in the surface concentration of tricarbonyl species but rather due to an increase of dicarbonyl and/or monocarbonyl species. The former is evident from the parallel increase of the intensity of the 2008 cm^{-1} band (band 4), representing the asymmetric stretching of dicarbonyl species. Nevertheless, it is also possible that part of the intensity increase of the 2075 cm^{-1} band is due to the monocarbonyl species.

In contrast, on Ru/SiO_2 the peak area of the HF_1 band increases by approximately 40% with an increase in temperature to 110 °C, suggesting in this case an increase in the surface concentration of the tricarbonyl species, either isolated or residing on RuO. This can account partially for the intensity increase of the 2075 cm^{-1} band. The additional increase can be attributed to monocarbonyl species adsorbed on Ru^{n+} sites, as indicated by the substantial increase in the intensity of band 7. Finally, the increase in intensity of band 3 in the 2010−2020 cm^{-1} region can be attributed to an increase in the surface concentration of isolated monocarbonyl species adsorbed on Ru sites surrounded by Ru^{n+} because of the increase of Ru^{n+} sites at elevated temperatures.

On both supports, a temperature is reached, after which the intensity of all bands in the 1950−2160 cm^{-1} region dropped drastically, presumably because of the onset of the CO oxidation reaction. The temperature at which this transition occurred is lower on Ru/SiO_2 (i.e., 210 °C) than on Ru/Al_2O_3 (i.e., 250 °C), presumably because of the lower stability of the adsorbed CO species on Ru/SiO_2, which appears to favor the CO oxidation reaction.[20] The apparent onset of CO oxidation is accompanied by an increase of the surface concentration of bridged species, as indicated by the intensities of the bands at 1865 cm^{-1} on Ru/Al_2O_3 and 1872 cm^{-1} on Ru/SiO_2. This increase is more pronounced in the case of Ru/SiO_2, probably because of the larger Ru particle size. These results are consistent with previous literature reports that indicate that lower surface coverages at higher temperatures favor the formation of bridged CO species.[18]

5. Conclusions

FTIR studies were used to examine the CO adsorption and desorption behavior on Ru supported on Al_2O_3 and SiO_2. Similar adsorbed species are formed in both cases, although there are differences in their surface concentrations, as indicated by the differences in the relative intensities of the individual bands observed. Fitting of the spectra obtained indicates the presence of a total of 11 bands in the case of Ru/Al_2O_3 and 10 bands in the case of Ru/SiO_2. These bands correspond to different adsorbed species, including monocarbonyl, dicarbonyl, and tricarbonyl species adsorbed on Ru sites with different oxidation states. Among these species, the linearly adsorbed CO on metallic Ru^0 sites is the most abundant on both catalysts. Although the bands observed on both samples are similar with only slight variations in their positions, the stabilities of the adsorbed species are quite different. Overall, the analogous CO species adsorbed on Ru/Al_2O_3 are more stable than those adsorbed on Ru/SiO_2, with the most stable species observed being a dicarbonyl adsorbed on metallic Ru, (i.e., $Ru^0(CO)_2$) on Al_2O_3.

In the presence of O_2, when the Ru surface becomes more oxidized at elevated temperatures, formation of dicarbonyl species on Ru^{n+} sites is favored on Ru/Al_2O_3, whereas formation of monocarbonyl species on Ru^{n+} sites is favored on Ru/SiO_2. These differences can be attributed to differences in particle sizes of Ru on the two supports. Finally, the lower stability of the CO species on Ru/SiO_2 appears to make them more reactive toward O_2, as evident by the lower ignition temperature of CO oxidation in this case.

Acknowledgment. We acknowledge partial financial support by the University of South Carolina NSF-I/UCRC Fuel Cell Center and useful discussions with Dr. Oleg S. Alexeev and Dr. Michael Myrick.

References and Notes

(1) Sheppard, N.; Nguyen, T. T. *Adv. Infrared Raman Spectrosc.* **1978**, *5*, 67.
(2) Hadjiivanov, K.; Lavalley, J.-C.; Lamotte, J.; Mauge, F.; Saint-Just, J.; Che, M. *J. Catal.* **1998**, *176*, 415.
(3) Kevin Kuhn, W.; He, H. W.; Goodman, D. W. *J. Vac. Sci. Technol.* **1992**, *101*, 2477.
(4) Brown, M. F.; Gonzalez, R. D. *J. Phys. Chem.* **1976**, *80*, 1731.
(5) Chen, H.-W.; Zhong, Z.; White, J. M. *J. Catal.* **1984**, *90*, 119.
(6) Dalla Betta, R. A. *J. Phys. Chem.* **1975**, *79*, 2519.
(7) Yokomizo, G. H.; Louis, C.; Bell, A. T. *J. Catal.* **1989**, *120*, 1.
(8) Davydov, A. A.; Bell, A. T. *J. Catal.* **1977**, *49*, 332.
(9) Robbins, J. L. *J. Catal.* **1989**, *115*, 120.
(10) Kuznetsov, V. L.; Bell, A. T.; Yermakov, Y. I. *J. Catal.* **1980**, *65*, 374.
(11) Lei, G.-D.; Kevan, L. *J. Phys. Chem.* **1991**, *95*, 4506.
(12) Uchiyama, S.; Gates, B. C. *J. Catal.* **1988**, *110*, 388.
(13) Solymosi, F.; Raskó, J. *J. Catal.* **1989**, *15*, 107.
(14) Zecchina, A.; Guglielminotti, E.; Bossi, A.; Camia, M. *J. Catal.* **1982**, *74*, 225.
(15) Guglielminotti, E.; Zecchina, A.; Bossi, A.; Camia, M. *J. Catal.* **1982**, *74*, 240.
(16) Guglielminotti, E. *Langmuir* **1986**, *2*, 812.
(17) Landmesser, H.; Miessner, H. *J. Phys. Chem.* **1991**, *95*, 10544.
(18) Beck, A.; Dobos, S.; Guczi, L. *Inorg. Chem.* **1988**, *27*, 3220.
(19) Abhivantanaporn, P.; Gardner, R. A. *J. Catal.* **1984**, *90*, 119.
(20) Chin, S. Y.; Alexeev, O. S.; Amiridis, M. D. *Appl. Catal.* **2005**, *286*, 157.
(21) Elmasides, C.; Kondarides, D. I.; Grünert, W.; Verykios, X. E. *J. Phys. Chem. B* **1999**, *103*, 5227.
(22) Todorova, S. Z. H.; Kadinov, G. B. *Res. Chem. Intermed.* **2002**, *28*, 291.
(23) Bond, G. C.; Slaa, J. C. *J. Mol. Catal A: Chem.* **1995**, *96*, 163.
(24) Coq, B.; Crabb, E.; Warawdekar, M.; Bond, G. C.; Slaa, J. C.; Galvagno, S.; Mercadante, L.; Ruiz, J. G.; Sierra, M. C. S. *J. Mol. Catal.* **1994**, *92*, 107.
(25) Bond, G. C.; Slaa, J. C. *J. Mol. Catal.* **1994**, *89*, 221.
(26) Wellenbüscher, J.; Muhler, M.; Mahdi, W.; Sauerlandt, U.; Schütze, J.; Ertl, G.; Schlögl, R. *Catal. Lett.* **1994**, *25*, 61.
(27) Pfnür, H.; Menzel, D.; Hoffmann, F. M.; Ortega, A.; Bradshaw, A. M. *Surf. Sci. Catal.* **1980**, *93*, 431.
(28) Zubkov, T.; Morgan, G. A., Jr.; Yates, J. T., Jr.; Kühlert, O.; Lisowski, M.; Schillinger, R.; Fick, D.; Jänsch, H. *J. Surf. Sci.* **2003**, *526*, 57.
(29) Nawdali, M.; Bianchi, A. *Appl. Catal., A* **2002**, *231*, 45.
(30) Mizushima, T.; Tohji, K.; Udagawa, Y.; Ueno, A. *J. Phys. Chem.* **1990**, *94*, 4980.
(31) Kantcheva, M.; Sayan, S. *Catal. Lett.* **1999**, *60*, 27.
(32) Benedetti, E.; Braca, G.; Sbrana, G.; Salvetti, F.; Grassi, B. *J. Organomet. Chem.* **1972**, *37*, 361.
(33) Johnson, B. F.; Johnston, R. D.; Josty, P. L.; Lewis, J.; Williams, G. *Nature (London)*, **1967**, 902.
(34) de Ménorval, L.-C; Chaqroune, A.; Coq, B.; Figueras, F. *J. Chem. Soc., Faraday Trans.* **1997**, *93*, 3715.
(35) Platero, E. E.; de Peralta, F. R.; Parra, J. B. *J. Eur. Ceram. Soc.* **1998**, *18*, 1307.
(36) Kellner, C. S.; Bell, A. T. *J. Catal.* **1981**, *71*, 296.
(37) Zhang, Z. L.; Kladi, A.; Verykios, X. E. *J. Mol. Catal.* **1994**, *89*, 229.
(38) McQuire, M. W.; Rochester, C. H. *J. Catal.* **1995**, *157*, 396.
(39) Bossi, A.; Garbassi, F.; Orlandi, A.; Petrini, G.; Zanderighi, L. *Stud. Surf. Sci. Catal.* **1978**, *3*, 405.
(40) Blanchard, G.; Charcosset, H.; Chenebauz, M. T.; Primet, M. *Stud. Surf. Sci. Catal.* **1978**, *3*, 197.